JCI insight

RESEARCH ARTICLE

A hyperthermic seizure unleashes a surge of spreading depolarizations in *Scn1a*-deficient mice

Isamu Aiba, Yao Ning, and Jeffrey L. Noebels

Department of Neurology, Baylor College of Medicine, Houston, Texas, USA.

Spreading depolarization (SD) is a massive wave of cellular depolarization that slowly migrates across the brain gray matter. Cortical SD is frequently generated following brain injury, while less is understood about its potential contribution to genetic disorders of hyperexcitability, such as *SCN1A*-deficient epilepsy, in which febrile seizure often contributes to disease initiation. Here we report that spontaneous SD waves are predominant EEG abnormalities in the *Scn1a*-deficient mouse (*Scn1a*$^{+/R1407X}$) and undergo sustained intensification following a single hyperthermic seizure. Chronic DC-band EEG recording detected spontaneous SDs, seizures, and seizure-SD complexes in *Scn1a*$^{+/R1407X}$ mice but not WT littermates. The SD events were infrequent, while a single hyperthermia-induced seizure robustly increased SD frequency over 4-fold during the initial postictal week. This prolonged neurological aftermath could be suppressed by memantine administration. Video, electromyogram, and EEG spectral analysis revealed distinct neurobehavioral patterns; individual seizures were associated with increased motor activities, while SDs were generally associated with immobility. We also identified a stereotypic SD prodrome, detectable over a minute before the onset of the DC potential shift, characterized by increased motor activity and bilateral EEG frequency changes. Our study suggests that cortical SD is a pathological manifestation in *SCN1A*-deficient epileptic encephalopathy.

Introduction

Spreading depolarization (SD) is a massive self-regenerative wave of sustained near-complete cellular depolarization slowly propagating across brain gray matter (1, 2). The profound cellular depolarization leaves prolonged hypoperfusion and depression of spontaneous neuronal activity, contributing to neurological dysfunction of variable severity depending on genetic, humoral, and physiological predispositions. SD is frequently generated in patients after brain injury and is associated with acute and chronic neurological deficits (2, 3). SD is also associated with visual and motor deficits in some genetic migraine with aura syndromes (4), and experimental studies suggest that repetitively provoked SD in healthy brain can produce migraine comorbidities such as photosensitivity, hyperalgesia, and anxiety (5, 6). There is a growing interest in understanding SD generation mechanisms, their neuropathological consequences, and therapeutic interventions.

Because of their excitatory nature, SD events are detected in association with seizures or epileptic discharges in both experimental and clinical settings (7, 8). These "peri-ictal" SD events have been considered as a candidate mechanism contributing to epilepsy comorbidities such as peri-ictal migraine headache and immobility (9), and the appearance of SD in subcortical structures correlates with cardiovascular and respiratory dysfunction linked to postictal mortality in experimental animal studies (10–12). SD generation patterns vary depending on the pathological context. In acutely injured brains, isolated seizures, SD, and seizure-SD complexes coexist in some patients, while some show only a seizure or SD pattern, suggesting independent thresholds for these depolarizing events (13). Whereas recurrent spontaneous seizures define epilepsy, the characterization of SD incidence in epilepsy, especially in cases without physical injuries, is extremely limited, since the DC potential shift is difficult to detect with human scalp EEG recording of filtered signals. The advance of defined monogenic mouse models of epilepsy offers the opportunity to circumvent this limitation.

Mutations in ion channel genes are a common cause of developmental epileptic encephalopathy (DEE) (14, 15), and both gain- and loss-of-function mutations in the *SCN1A*/Nav1.1 gene are identified across a range of DEE phenotypes (16). *Scn1a*/Nav1.1 channels are widely expressed in both human and rodent

Conflict of interest: The authors have declared that no conflict of interest exists.

Submitted: March 13, 2023
Accepted: June 15, 2023
Published: August 8, 2023

Reference information: *JCI Insight*. 2023;8(15):e170399. https://doi.org/10.1172/jci.insight.170399.

neocortices (17–19). However, their dysfunction preferentially impacts specific neuronal populations, such as fast-spiking inhibitory neurons owing to their predominant reliance on *Scn1a*/Nav1.1-containing channels (20–22). Gain-of-function *SCNA1* mutations have been identified in rare genetic DEE and familial hemiplegic migraine type 3 (FHM3) patients (23, 24), and increased SD susceptibility has been reported in the knockin mouse models (25, 26). The more common *SCN1A* loss-of-function mutations are associated with epileptic encephalopathies (e.g., Dravet syndrome) with a range of severity partly reflecting the severity of mutation (27). In these cases, reduced inhibitory neuron excitability results in network synaptic disinhibition and the emergence of hyperexcitable neuronal circuitry (20) and high susceptibility to hyperthermia dependent seizures that are believed to initiate and exacerbate epileptic encephalopathy (28). It is not known whether cortical SD is involved in the pathophysiological phenotype of this loss-of-function sodium channelopathy.

In this study, we identified the spontaneous incidence of SD in adult *Scn1a*$^{+/R1407X}$ (hereafter *Scn1a*$^{+/RX}$) mice using DC-band cortical EEG recording. During prolonged monitoring studies, we found that spontaneous SDs were profoundly increased in the aftermath of a single hyperthermic seizure, and the effect was partially mimicked by a single subconvulsive pentylenetetrazole stimulation. The exacerbation persisted for up to a week and was mitigated by concurrent administration of memantine. We also established that these SD events are not purely electrographic but affect spontaneous behaviors; cortical detection of SD is preceded by a brief period of motor hyperactivity accompanied by a high-frequency shift of EEG activity and followed by behavioral arrest and EEG suppression. Together, our study reveals a pathophysiological phenotype of *SCN1A*-deficient encephalopathy and suggests SD as a potential and targetable contributor to comorbidity mechanisms in this disorder.

Results

Chronic monitoring of spontaneous cortical SD and seizures in Scn1a-deficient mice. We characterized SD incidence in *Scn1a*-deficient (*Scn1a*$^{+/RX}$) and WT mice using a DC-band chronic EEG recording method reported in our previous study (8). In the study cohorts, we recorded a total of 17 *Scn1a*$^{+/RX}$ (7 male, 10 female) and 11 littermate WT mice (5 male and 6 female) from a total of 13 litters. Recordings started at the age of P40–P96. After 7 days of baseline recordings, mice were subjected to a single hyperthermic seizure (details described below), and the effect was monitored for 10 days.

The results are summarized in Figure 1. We detected 3 abnormal baseline spontaneous events: isolated SD, seizures, and complexes of seizure with postictal SD (hereafter "seizure+SD") in which an SD emerged within minutes following a seizure (Figure 1, A–E). During the study, one *Scn1a*$^{+/RX}$ mouse died during hyperthermic seizure, and 6 mice died due to postictal sudden death or moribund condition (Figure 1F). While the baseline incidence of seizures and SD was relatively rare (mean of both events 0.57 ± 0.35 per day), SD was detected more commonly than seizures in most mice (Figure 1, H and I). No seizures or SD were detected in WT mice during the baseline or posthyperthermia periods (Figure 1F).

After 7 days of baseline recording, mice were subjected to a hyperthermic seizure (see Methods), and its effect was continuously monitored for more than 10 days. Starting 1 day after the posthyperthermic seizure, SD frequency clearly increased in *Scn1a*$^{+/RX}$ mutants (Figure 1, F and G), even in 2 mice that had not shown any seizure or SD during baseline recording. This upsurge in SD frequency lasted for multiple days and up to a week, rendering SD the dominant abnormal EEG event (Figure 1H). Statistical analyses detected significant increases in the frequencies of spontaneous SD (4.2-fold) and total events (3.3-fold) following the hyperthermic seizure (Figure 1I). In the 2 exceptional "seizure-only" mice that did not show SD during baseline nor during the hyperthermic seizure, seizure frequency decreased after the hyperthermic seizure. Because of the rare chance to encounter them, we could not specifically analyze more of these mice. In a time-control study in which 5 *Scn1a*$^{+/RX}$ mice were continuously monitored without induction of hyperthermic seizure, no significant difference in seizure/SD frequency was detected (data not shown).

There was a weak diurnal trend in the SD frequency in this monitoring cohort, with peaks detected at 6.5 hours and 17.8 hours, which correspond to light-dark cycle transitions (Figure 1J). A similar circadian sudden unexpected death in epilepsy (SUDEP) mortality pattern was previously detected in the same *Scn1a*-deficient mouse model (29), implying the presence of a circadian vulnerability in this mutant mouse model.

High SD susceptibility during the hyperthermic seizure in Scn1a$^{+/RX}$ *mice*. In addition to its high spontaneous incidence, SD generation was also common during hyperthermic seizure in *Scn1a*$^{+/RX}$ mice. Following heat exposure, *Scn1a*$^{+/RX}$ mice showed cortical spikes and sialorrhea (drooling) as the body core temperature approached 40°C. Seizure onset in *Scn1a*$^{+/RX}$ always coincided with a vocalization followed by a generalized

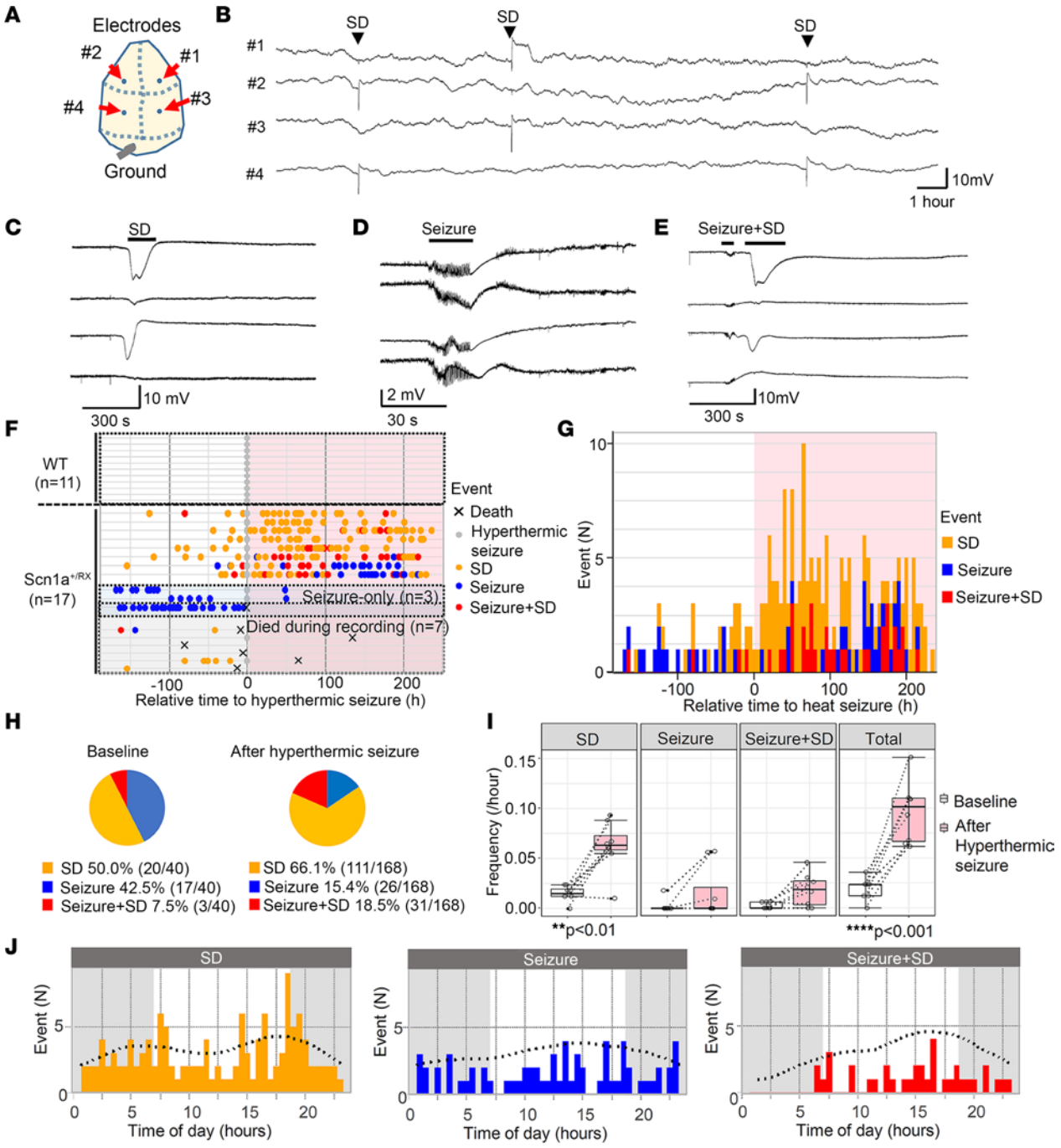

Figure 1. Seizure and SD phenotype of *Scn1a*$^{+/RX}$ mice before and after a hyperthermic seizure. (**A**) Electrode positions: from the top, #1 right anterior, #2 left anterior, #3 right posterior, #4 left posterior. (**B**) Compressed trace showing a 24-hour recording. SDs are reliably detected as sharp negative shift over stable baseline. (**C**–**E**) Expanded representative traces of SD, seizure, and seizure+SD complex. (**F**–**H**) Hyperthermic seizure robustly increased SD and seizure incidence. (**F**) Raster plots of seizure and SD incidence in WT and *Scn1a*$^{+/RX}$ mice. WT mice had no seizure or SD. Three mice exclusively had seizures ("seizure-only"). Seven mice died or became moribund during the study. The same *Scn1a*$^{+/RX}$ event data are presented in a cumulative histogram (**G**) and pie chart (**H**) showing proportion of seizure, SD, and seizure+SD events during baseline and after a hyperthermic seizure in *Scn1a*$^{+/RX}$ mice that survived the recording period, excluding the "seizure-only" mice. (**I**) Quantification of event frequencies. Frequencies of SD and total events were increased after a hyperthermic seizure. "Seizure-only" mice were excluded from this analysis. Two-way ANOVA and post hoc Tukey's test. (**J**) Chronological analysis of SD, seizure, and seizure+SD events.

tonic clonic seizure, and was electrographically detected as a train of ictal spiking that resulted within less than 1 minute in a temporally coupled SD (Figure 2A). Mice are usually unconscious or semiconscious during the minutes-long postictal period. SD was detected in 77% (10/13) of the *Scn1a*$^{+/RX}$ mice during hyperthermic seizure induction (Figure 2C) and was usually associated with postictal loss of voluntary motor behavior and an occasional myoclonic jerk. SD always appeared after the electrographic seizure and was likely generated as a secondary consequence of neuronal discharges, while brain hyperthermia might facilitate it. The 3 *Scn1a*$^{+/RX}$ mice that did not display SD during hyperthermic seizure were "seizure-only" mice, and 1 of these died shortly after this period. In WT mice, ictal SD was less common during the hyperthermic period (27% [3/11], $P = 0.037$ vs. *Scn1a*$^{+/RX}$, Fisher's exact test; Figure 2, B and C). Consistent with earlier studies (30), the hyperthermic seizure threshold was significantly higher in WT littermates (WT: 43.0°C ± 1.0°C, $n = 11$; *Scn1a*$^{+/RX}$: 41.7°C ± 0.7°C, $n = 12$; $P = 0.007$, Mann-Whitney test), which also required longer heat exposures (>30 minutes) until a seizure emerged (Figure 2D).

Hyperthermic seizure does not modulate the kinetics of individual seizure or SD. Hyperthermia modulated the number but not the localization or kinetics of individual SD and seizure events. We detected a total of 160 SDs, 95 seizures, and 43 seizure+SD complexes. Regardless of the presence or absence of a preceding seizure, almost all SDs were serially detected first with the posterior and next with the anterior electrode (isolated SD: 99% [159/160]; seizure+SD: 98% [42/43]). While all seizures were detected as bilaterally generalized events, SDs were always unilateral and tended to be detected more often in the left than the right hemisphere (SD: left 97 vs. right 63, $P = 0.072$; seizure+SD: left 26 vs. right 17, $P = 0.39$; Fisher's exact test). These characteristics suggest the presence of a stereotypic SD generation mechanism in *Scn1a*$^{+/RX}$ mice (see Discussion).

Postictal generalized EEG suppression (PGES) is a simultaneous silencing of EEG activity across all electrodes immediately following a generalized seizure, and its presence and duration often correlate with the clinical severity of postictal deficits (31, 32). While its origin is uncertain, the loss of EEG amplitude could resemble the consequence of SD. However, in this model, PGES period could be distinguished from the SD-dependent EEG depression (Figure 3A). In 47% (20/43) of seizure+SD complexes, we detected PGES lasting for 13.9 ± 5.0 seconds, and neither PGES incidence nor duration differed after a seizure with or without postictal SD (Figure 3, B and C). Thus PGES in this mouse model is a separable process that did not seem to predict or correlate with postictal SD incidence. The relatively small EEG suppression after spontaneous SD in awake mice is consistent with our earlier study (8) and likely reflects the higher spontaneous brain activity compared with anesthetized preparations.

Based on the increased spontaneous SD event frequency shown in Figure 1D, hyperthermic seizure might be expected to facilitate postictal SD generation by shortening the time to onset. However, the latency to postictal SD was significantly prolonged after hyperthermic seizure (Figure 3D). Hyperthermic seizure did not alter the kinetics of individual events; thus no differences were detected in SD durations (baseline: 75.2 ± 24.7 seconds, $n = 39$; after hyperthermic seizure: 72.1 ± 21.2 seconds, $n = 121$; $P = 0.70$), SD amplitudes (baseline: 9.4 ± 2.4 mV, $n = 39$; after hyperthermic seizure: 8.9 ± 2.4 mV, $n = 121$; $P = 0.18$), seizure durations (baseline: 42.9 ± 13.3 seconds, $n = 44$; after hyperthermic seizure: 41.9 ± 12.9 seconds, $n = 51$; $P = 0.63$), or seizure amplitudes (baseline: 2.3 ± 0.70 mV, $n = 44$; after hyperthermic seizure: 2.5 ± 0.80 mV, $n = 51$; $P = 0.46$). Overall, hyperthermic seizure seems to affect only the event generation pattern (event frequency, latency of postictal SD onset), not the individual event severity.

In contrast, the kinetics of SD and seizure activities detected in seizure+SD complexes differ from those detected individually. The duration of SDs in seizure+SD complexes was significantly shorter than that of SDs detected without a preceding seizure (isolated SD duration: 72.9 ± 21.8 seconds; SD in seizure+SD: 61.3 ± 22.6 seconds; $P < 0.0001$; Figure 3E). Similarly, seizure duration was also shorter when detected in a seizure+SD complex (duration: isolated seizure 41.5 ± 13.5 seconds vs. seizure in seizure+SD 28.6 ± 9.6 seconds, $P < 0.0001$; Figure 3G). On the other hand, the peak amplitudes of negative DC offset during SD and seizure were unchanged (Figure 3, F and H).

These analyses highlight the qualitative differences between seizure and SD components in a seizure+SD complex compared with those detected individually.

Memantine administration suppresses the prolonged aftermath of a hyperthermic seizure. We next examined whether pharmacological inhibition using the NMDAR antagonist memantine might attenuate the depolarizing aftermath of a hyperthermic seizure, since NMDAR activation has been implicated in a model of febrile seizure–induced epileptogenesis (33). Memantine is an FDA-approved NMDAR antagonist, and its

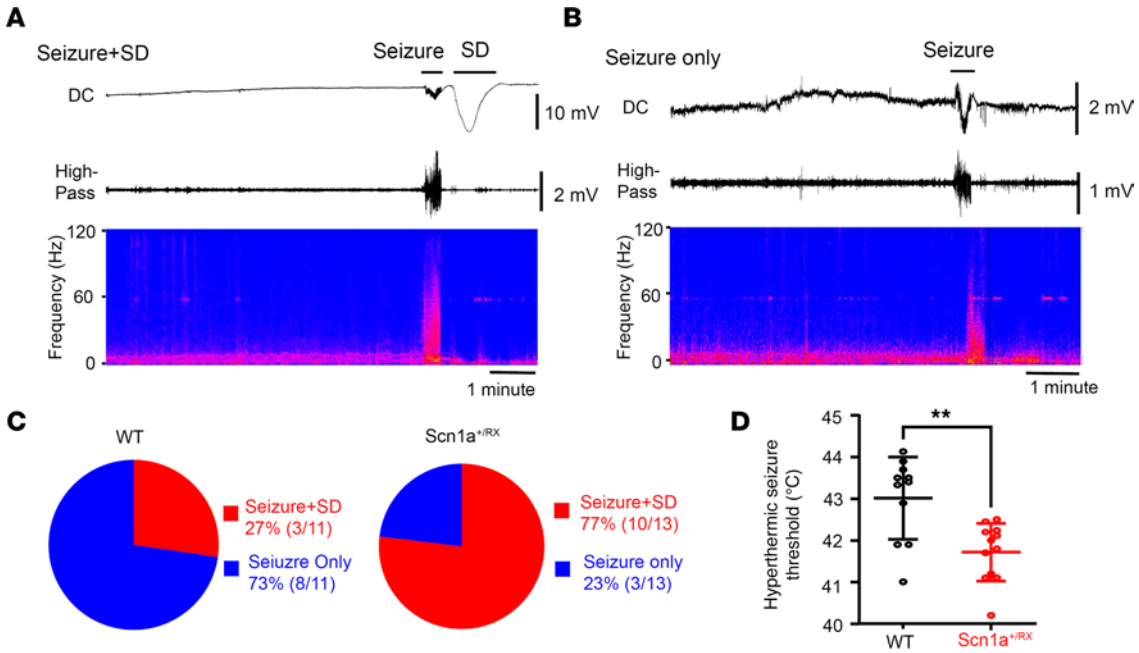

Figure 2. SD generation during hyperthermic seizures induced with a heating lamp in *Scn1a*$^{+/RX}$ mice. (**A** and **B**) Representative EEG showing seizure and SD. Top: DC; middle: high pass (>1 Hz); bottom: power spectrum of EEG (anterior electrode). (**C**) Postictal SD was less common in WT mice: 77% (10/13) of *Scn1a*$^{+/RX}$ mice developed SD following seizure, while 27% (3/11) of WT mice did so. (**D**) Consistent with previous studies, *Scn1a*$^{+/RX}$ mice showed a lowered thermal threshold for seizure. WT: $n = 11$; *Scn1a*$^{+/RX}$: $n = 13$; $P = 0.007$, Mann-Whitney U test. $^{**}P < 0.01$.

rapid absorption and relatively short half-life in mouse brain (~4 hours; ref. 34) proved useful in analyzing the temporal contribution of NMDAR to hyperthermic seizure–induced SD exacerbation. We selected 10 mg/kg (i.p.), a dose that inhibits an NMDAR-dependent plasticity mechanism in vivo (35), and used different administration patterns to investigate critical time windows: pretreatment (30–60 minutes before the hyperthermic seizure), posttreatment (6 and 16 hours after hyperthermic seizure induction), and a combined pre/posttreatment. The drug effect was evaluated by comparison of the frequency of total events before and 24 hours after hyperthermic seizure induction. The initial 24-hour postictal period was excluded from the analysis to avoid the acute proconvulsive effect of prolonged memantine administration. In fact, 2 mice in pre/posttreatment group showed a recurrent seizure during memantine administration (Figure 4D; see Discussion).

Memantine at high dosage is known to acutely inhibit SD generation in some models (36). We found that pretreatment with memantine was partially effective at inhibiting SD generation during hyperthermia seizure; SD incidence in memantine-pretreated mice (i.e., pre- and pre/posttreated mice) was 56% (9/16 mice), which is less than in untreated mice (untreated control plus posttreated mice, 88% [14/16 mice], $P = 0.052$, Fisher's exact test). Memantine administration inhibited the chronic aftermath of hyperthermic seizure (2-way ANOVA; memantine administration paradigm: $F = 1.68$, $P = 0.18$; time effect: $F = 5.74$, $P = 0.020$; interaction: $F = 2.63$, $P = 0.060$). All mice receiving saline before hyperthermic seizure showed a robust increase in the total number of events ($P = 0.014$; Figure 4A). In this control cohort, more mice later developed seizures compared with the initial cohort shown in Figure 1. A significant increase in total events was also seen in the pretreatment group ($P = 0.030$; Figure 4B), while the aftermath was absent in 1 mouse. Memantine treatment initiated after hyperthermic seizure attenuated the aftermath ($P = 0.23$; Figure 4C), although the total number of seizure/SD events was still increased in 75% (6/8) of mice. The combined pre/posttreatment was most effective, as the frequencies of the seizure/SD events were unchanged or decreased during the posthyperthermic seizure period in all mice tested ($P = 0.10$; Figure 4D).

These results collectively suggest that continuing NMDAR activation after hyperthermic seizure contributes to the exacerbation of depolarizing phenotype of *Scn1a*$^{+/RX}$ mice.

Subconvulsive pentylenetetrazole partially mimics the effect of hyperthermic seizure. The contribution of NMDAR activity raised a possibility that the prolonged increase in spontaneous SD incidence following a hyperthermic seizure might be explained by subthreshold circuit hyperexcitation. This possibility was tested

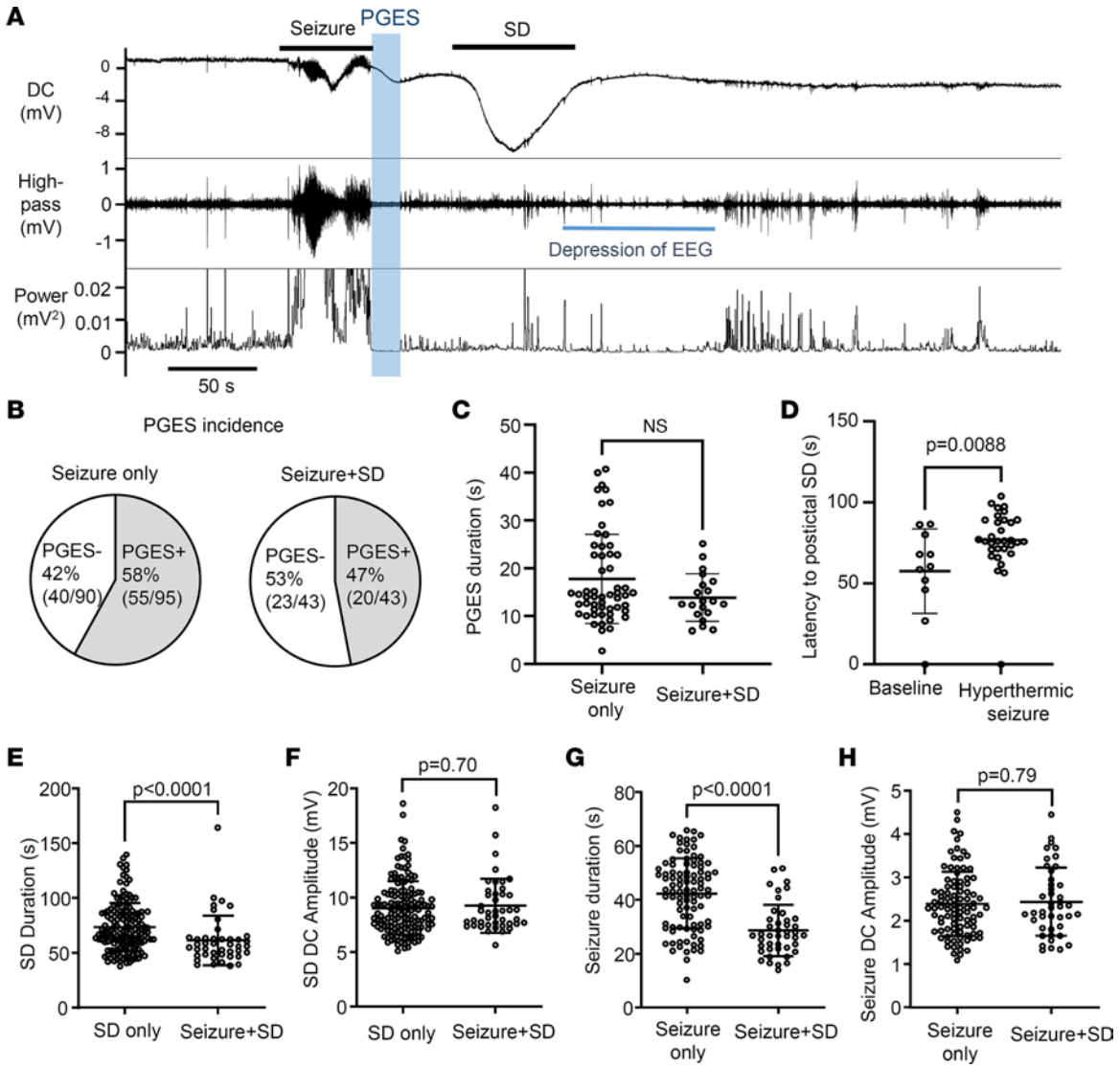

Figure 3. Electrophysiological characteristics of PGES and postictal SD. (**A**) Representative trace showing the temporal sequence of PGES (depressed EEG amplitude, blue window) and postictal SD generation. Top: DC; middle: high pass (>1 Hz); bottom: EEG converted into power. (**B** and **C**) The PGES incidence (**B**) and duration (**C**) were similar in seizure without postictal SD and seizure with postictal SD. Seizure only: *n* = 55; seizure+SD: *n* = 20. (**D**) The latency to SD after seizure termination is significantly prolonged after a hyperthermic seizure. Baseline: *n* = 11; after hyperthermic seizure: *n* = 32. (**E**–**H**) Comparison of seizure/SD kinetics between those in isolated events and those in the seizure+SD complex. The duration of SD in the seizure+SD complex is shorter than the duration of SD detected alone (**E**), while the DC amplitudes were not different (**F**). Similarly, the duration of seizure in the seizure+SD complex is shorter than the duration of seizure that appeared without SD (**G**), while the DC amplitudes were not different (**H**). SD only: *n* = 160; seizure only: *n* = 95; seizure+SD: *n* = 43. Statistics were computed by Mann-Whitney *U* test.

by a single injection of pentylenetetrazole (PTZ), a convulsant that acts as a GABA-A receptor antagonist. After baseline recordings, 7 *Scn1a*$^{+/RX}$ mice were injected with PTZ (30 mg/kg, i.p.), a dosage considered subconvulsive in WT mice (ED_{50} ~65 mg/kg; ref. 37). Although the half-life of PTZ in the mouse brain is not available, it is estimated to be less than 2 hours based on the analysis in dogs (38) as well as the time course of appearance of PTZ-provoked epileptic spikes in our recordings. Thus SD or seizure events appearing 2 hours after administration are considered secondary to the direct network excitation by PTZ.

Five mice showed recurrent ictal spikes without seizure or SD during the 2 hours after PTZ injection (Figure 5, A–C), while 2 mice showed a seizure immediately after PTZ injection and 1 of them died postictally. Continuous monitoring revealed enhanced recurrent SD/seizure frequencies for several days in 4 surviving mice (Figure 5, B and C), and there was a trend toward increase in the mean total seizure/SD events ($P = 0.0625$; Figure 5D). This result suggests that subconvulsive synaptic disinhibition is sufficient to produce a prolonged hyperexcitation profile of enhanced SD/seizure in *Scn1a*$^{+/RX}$ mice when NMDAR overactivation is present.

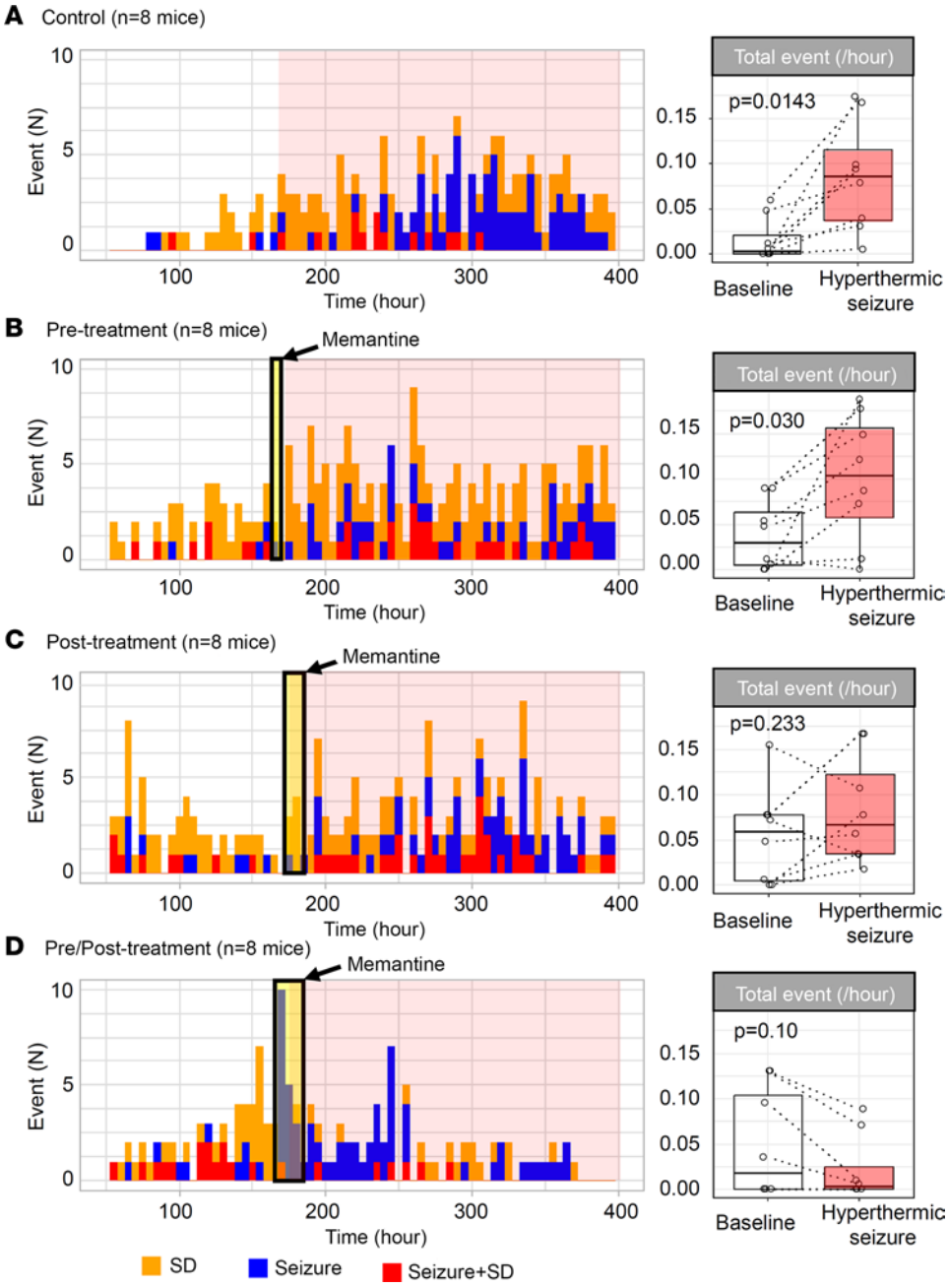

Figure 4. Prolonged memantine administration inhibits the hyperthermic seizure–induced exacerbation of depolarizing events in *Scn1a*$^{+/RX}$ mice. Cumulative histogram bars show SD incidence (orange), seizures (blue), and seizure+SD complexes (red) before and after hyperthermic seizure. Box plots show total event frequency (total events per hour) during baseline (white) and after hyperthermic seizure (red). (**A**) Pattern of events in saline-pretreated control *Scn1a* mutants. (**B**–**D**) Efficacy of single-dose memantine (10 mg/kg, i.p.) pretreatment administered 30–60 minutes before hyperthermic seizure (**B**), efficacy of memantine after treatment repeated 6 and 12 hours after hyperthermic seizure (**C**), and combined pre- and posttreatment data (**D**) were analyzed. The duration of treatment is shown in the yellow shade, and the duration of the posthyperthermic seizure period in the pink shade. At right, the frequency of total events during baseline and following the hyperthermic seizure is shown. In each group, *n* = 8 mice. Statistics calculated by paired Wilcoxon's signed-rank test.

Interictal and postictal motor activity associated with SD. We next sought to identify neurophysiological deficits associated with SD using chronic EEG with neck muscle electromyography (EMG). This analysis revealed stereotypical motor activity patterns accompanying interictal SD episodes, characterized by prodromal minutes-lasting motor activity prior to SD detection at the parietal electrode, followed by suppres-

sion of activity for minutes after SD was detected at the frontal electrode (Figure 6A). In contrast, seizures were associated with a robust EMG signal increase following the onset of EEG discharges (Figure 6B). In some mice, these convulsive EMG signals were transiently suppressed during PGES as reported in an electrically evoked seizure model (39), but were then followed by bursts of motor activity. During a seizure+SD complex, the seizure again triggered an initial sharp EMG activity burst, followed by a transient reduction once SD was detected at the frontal electrode (Figure 6C). In the majority of mice, EMG activity remained low after the postictal SD. Overall, seizure+SD showed lower postictal motor activity compared with seizure ($P < 0.001$, ANOVA of aligned rank-transformed data).

Decreased voluntary locomotor behavior is associated with SD. Locomotor behavior associated with seizure, SD, and seizure+SD events was analyzed using video recording. In total, 37 seizures, 67 SDs, and 14 seizure+SD complexes from 7 mice were analyzed after the removal of low-quality images. Average locomotion during a 30-minute period before and after each event type is presented in Figure 7A. Unlike EMG analysis (Figure 6B), this analysis did not detect behavior increase associated with isolated seizures, suggesting that increased ictal motor activities detected by EMG were mostly stationary jerking movements. As in EMG analysis, SD tended to be associated with decreases in locomotion minutes after SD, although the effect was less robust. Combined seizure+SD suppressed locomotion for a prolonged period.

Since the analysis of mean data could be biased by a few events with large activity, we also analyzed the locomotion using a binary method in which 5-second time bins are scored as "active" or "inactive" periods (see Methods). The binned analysis 5 and 10 minutes before and after event onset again revealed lower total activity associated with seizure+SD compared with seizure alone, while SD alone showed an intermediate level (Figure 7, B and C). Analysis of locomotion before and after each event did not show directional changes in seizure ($P = 0.21$) and SD ($P = 0.73$), while seizure+SD tended to reduce the subsequent locomotion ($P = 0.059$; Figure 7, D–F).

Together, these motor activity patterns suggest that SD episodes suppress voluntary motor behaviors as was previously observed in optogenetically evoked SD (40, 41).

Stereotyped EEG activity changes also precede the detection of negative DC potential shift in the cortex. Given the behavioral evidence of a neurological precursor signaling SD onset detected with EMG analysis, we examined EEG characteristics preceding the detection of a spontaneous cortical SD using 45 randomly selected events from 10 *Scn1a*$^{+/RX}$ mice. This analysis identified a striking signature preceding isolated SD episodes, characterized by a sudden and bilaterally simultaneous reduction in low-frequency (0–30 Hz) and increase in high-frequency (30–120 Hz) band EEG activity (hereafter termed pre-SD; $P < 0.0001$, both SD side and contralateral hemisphere; Figure 8A). These 2 frequency bands were selected based on multiple analyses to obtain robust characteristics with reproducibility and simplicity. During the pre-SD period, total EEG power (0–120 Hz) was reduced in both hemispheres as low-frequency activity dominated the baseline EEG power, while the decrease was slightly larger in the SD-affected hemisphere (pre-SD total EEG power relative to baseline: SD side 43.9% ± 20.0% vs. contralateral 47.5% ± 17%, $P = 0.039$, $n = 45$). This EEG power change occurred 87 ± 18 seconds before the negative DC shift onset, and was temporally correlated with the prodromal motor activity increase. The onset of the pre-SD phase was always associated with compound cortical spikes (Figure 8A, inset) detected in all cortical channels. This pre-SD EEG condition disappeared once the negative DC potential shift emerged.

A similar pattern of low-/high-frequency change was also detected in the pre-SD phase of seizure+SD ($P < 0.0001$, both SD side and contralateral, $n = 21$; Figure 8, B–D), although high-frequency activity did not change over the SD-affected side, partly because EEG activities in both low- and high-frequency bands were already depressed following a seizure in both hemispheres (pre-SD total EEG power relative to baseline: SD side 34.7% ± 18.0% vs. contralateral 39.1% ± 14.7%, $P = 0.16$).

Together, our analysis identified a clear electrobehavioral signature appearing more than a minute before cortical SD detection, likely reflecting the effect of SD generation and spread from a remote site. The EEG frequency shift and associated motor behavior changes may serve as a predictive biomarker signaling SD initiation in this model.

Discussion

In this study, we identified a spontaneous cortical SD generation phenotype in the *Scn1a*$^{+/RX}$ mouse model. SD episodes were readily detected in *Scn1a*-deficient mice, usually more frequently than seizures, and the incidence of SD was robustly increased after a single hyperthermic seizure, an effect that can last for days or a week. A

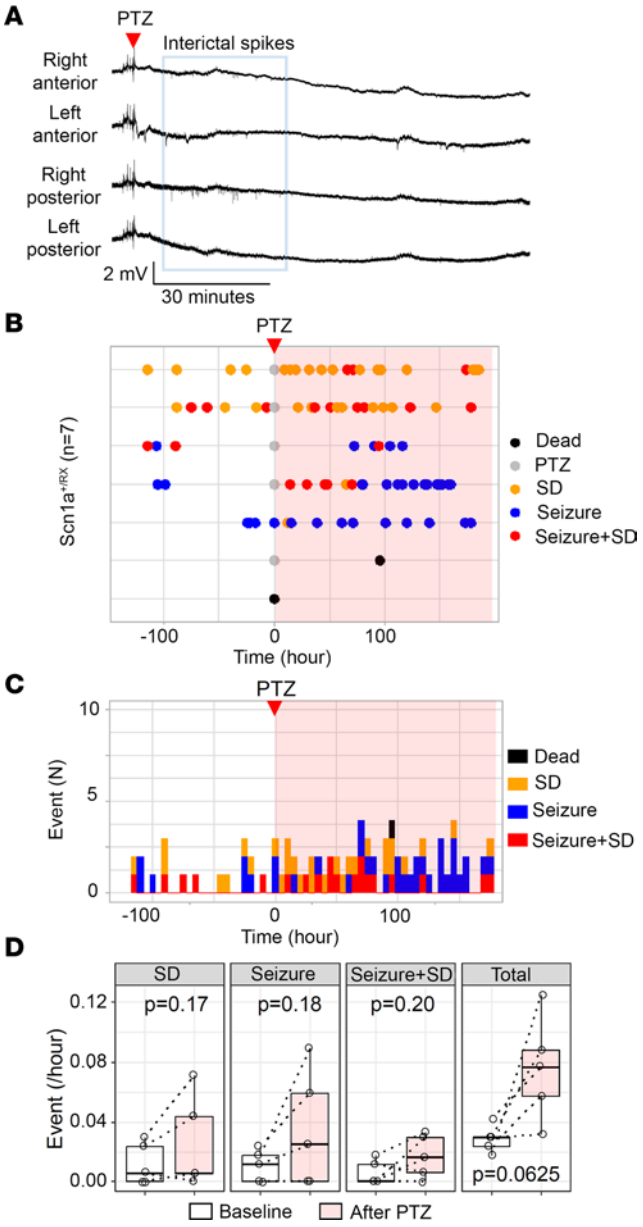

Figure 5. Subconvulsive PTZ stimulation partially mimics hyperthermic seizure effect. (**A**) Representative traces of EEG activity following PTZ injection (30 mg/kg, i.p.) in 7 *Scn1a*$^{+/RX}$ mice. PTZ increased interictal epileptic discharges for 30 minutes without seizure in this mouse. Traces from top: right anterior, left anterior, right posterior, left posterior. (**B**) Raster plots of SD, seizure, and seizure+SD complex during baseline and after PTZ injection (pink shade). Two mice died during the recording. (**C**) The same results presented in cumulative histogram of SD, seizure, and seizure+SD incidences. (**D**) Quantitative comparison of frequencies of SD, seizure, seizure+SD, and total events before and after PTZ injection. *n* = 5; statistics calculated by paired Wilcoxon's signed-rank test.

single subconvulsive dose of PTZ produced a similar upsurge. The posthyperthermia week-long flurry of SD events could be inhibited by memantine when administered immediately before and continuously after the hyperthermic seizure, suggesting that early and prolonged NMDAR activation may redundantly contribute to the prolonged aftermath. Simultaneous electrophysiological and behavioral characterization also revealed that seizures and seizure+SD complexes are qualitatively different and associated with distinct prodromal and postictal behavioral states. These short-term effects may herald more consequential behavioral and cognitive deficits reported in *Scn1a*-deficient mouse models (42–45). We have not analyzed younger age and cannot yet evaluate whether an early onset of SD might contribute to the developmental cognitive delay apparent in childhood Dravet syndrome. While our preclinical study suggests SD as a prominent pathological event associated

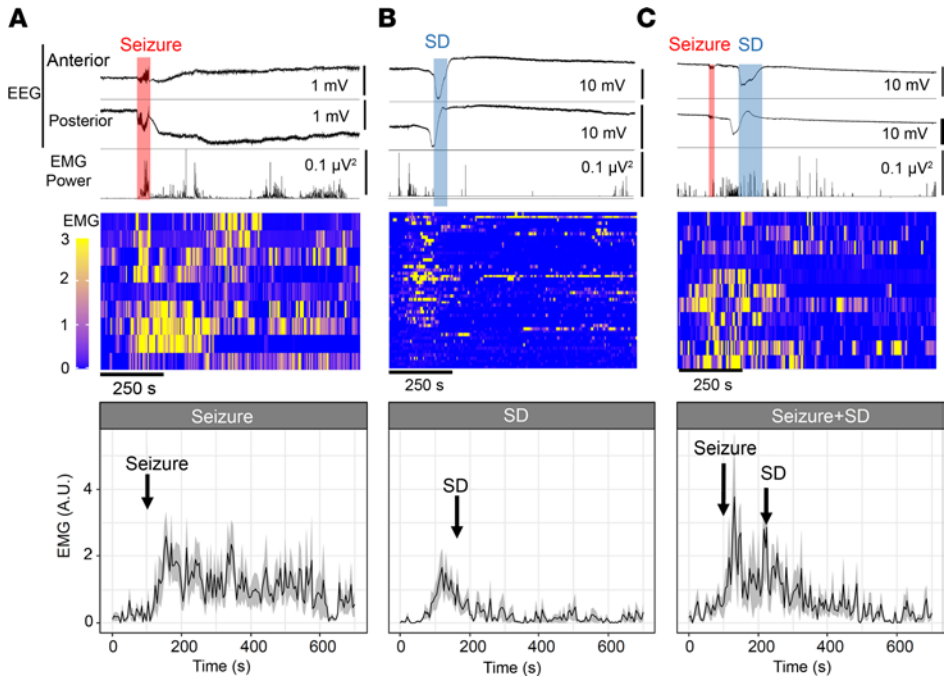

Figure 6. Analysis of EMG motor activity associated with SD, seizure, and seizure+SD. Top: Unilateral anterior and posterior EEG and simultaneous neck EMG trace. Middle: Raster plot of individual analyzed EMG signal patterns. Each lane represents a single event in a representative animal. Bottom: Averaged traces of EMG activity are presented as mean ± SEM. (**A**) Seizure is associated with an abrupt increase in EMG signal, which is followed by motor activations. (**B**) SD is associated with prodromal behavior activation, followed by suppression as DC shift is detected in the frontal cortex. (**C**) Seizure+SD is also associated with initial convulsive motor activity, which is inhibited once SD is detected over the frontal cortex. Some motor activity is present after postictal SD but is reduced in comparison with seizure alone. n = 11, 47, and 9 events for seizure, SD, and seizure+SD, respectively. $P < 0.001$ in EMG patterns between events, aligned rank transformation ANOVA.

with *Scn1a* deficiency, the overall clinical incidence and significance of SD in DEE remain uncertain owing to the difficulty of reliably detecting SD in human scalp EEG recordings. Further study will be required to determine whether the prodromal EEG activity we detected preceding SD initiation can potentially serve as a surrogate biomarker of SD occurrence. Alternative pharmacological SD may also help determine whether identification and early clinical management of SD will prove useful for predicting the emergence of clinical comorbidities in these individuals.

Spontaneous cortical SD characteristics of Scn1a-deficient mice. Our study revealed frequent spontaneous episodes of SD, rare seizure+SD complexes, and a prolonged period of high SD susceptibility following a hyperthermic seizure in the *Scn1a*$^{+/RX}$ mouse cortex. Throughout the study, no SD was detected during handling or in the presence of an investigator during the chronic monitoring; thus spontaneous SD detected here appears unlinked to potential experimental stress. Acute SD generation after a heat-induced seizure was previously documented in a 2-photon Ca^{2+} imaging study of immobilized *Scn1a*$^{+/-}$ mice (46), and our study extended the finding by demonstrating and analyzing in detail these spontaneous events and associated behavior comorbidities. Hyperthermia facilitates SD generation in brain-injured patients (47), and bath temperature above 38°C can trigger SD in isolated healthy hippocampus slices (48). This further underscores the higher SD susceptibility of *Scn1a*-deficient brain, since SD during hyperthermic seizure was more common in *Scn1a*$^{+/RX}$ than in WT mice despite the fact that their seizures were provoked at a lower body temperature than WT.

The neurophysiological mechanism underlying the high spontaneous SD susceptibility in *Scn1a*$^{+/RX}$ mice remains unclear, and the exact molecular pathogenesis is likely to be gene specific. In a model of type 2 familial hemiplegic migraine, spontaneous SD arises as a consequence of localized glutamate excess associated with genetically impaired astrocytes (49). This mechanism is unlikely to explain the pathogenesis of SD in the *Scn1a*-deficient mouse, where impaired GABAergic inhibition is the major mechanism of circuit hyperexcitation. We also observed that a network disinhibition by a subconvulsive dose of PTZ facilitated SD

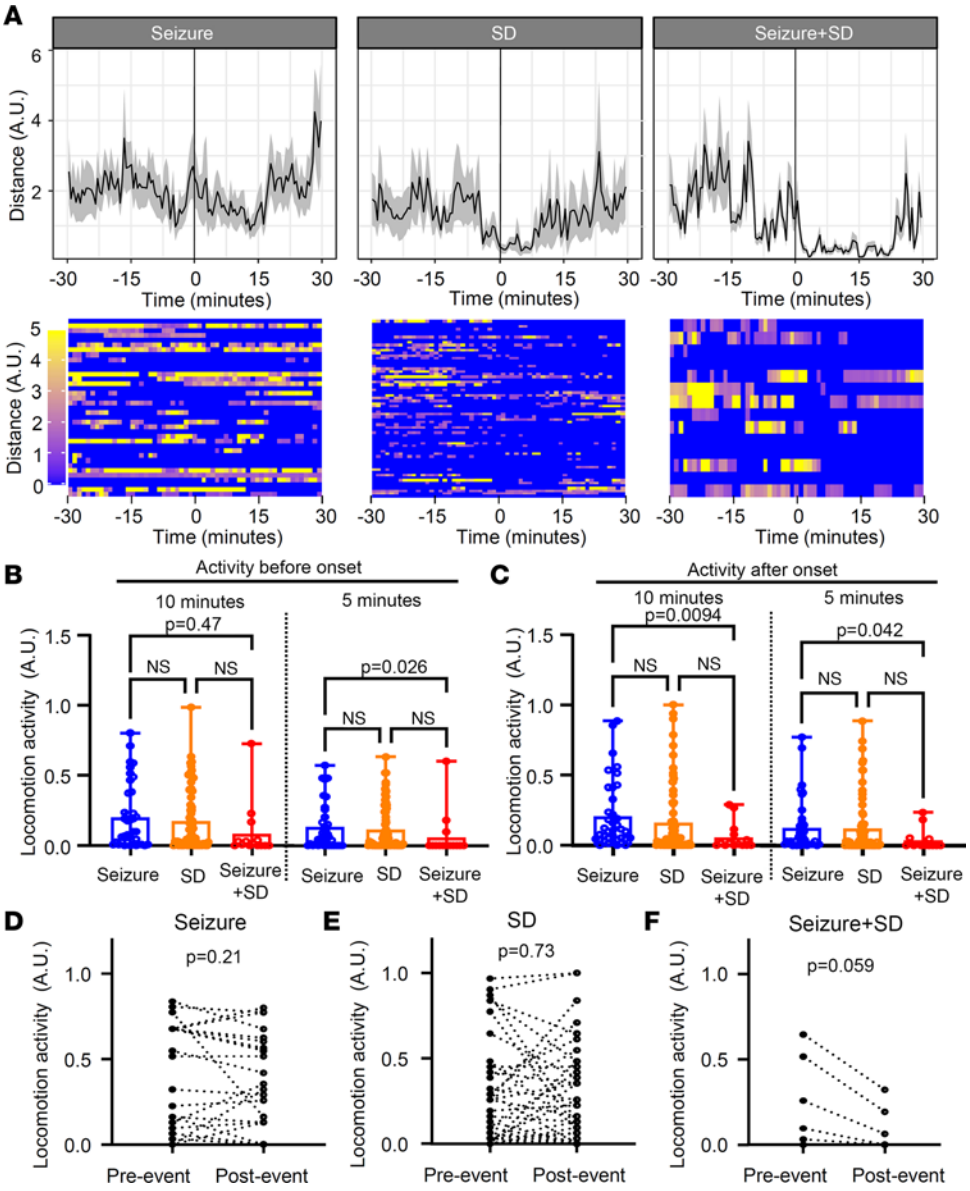

Figure 7. Locomotion changes associated with seizure, SD, and seizure+SD were analyzed using video images. (**A**) Average traces (top, mean ± SEM) and raster plots (bottom; each lane shows a single event) 30 minutes before and after event onset (line at $t = 0$). $n = 37$, 67, and 14 events for seizure, SD, and seizure+SD, respectively. (**B** and **C**) Locomotion was also analyzed by a binary method (see Results). Comparison of locomotion 10 or 5 minutes before (**B**) and after (**C**) each event. Seizure+SD is associated with reduced pre- and postevent locomotion activity. (**D**–**F**) Comparisons of locomotion changes in individual events 3 minutes before and after each event. Seizure and SD did not show consistent directional changes; however, seizure+SD events consistently reduced locomotion activity. Two-way ANOVA; event: $F = 2.01$, $P = 0.14$; time: $F = 15.93$, $P < 0.001$; interaction: $F = 1.23$, $P = 0.30$.

generation. In our study, SD was almost always sequentially detected with posterior to anterior electrodes, suggesting a stereotypic SD generation specific to the *Scn1a*-deficient network disinhibition. In this regard, characterization of SD phenotype in related epilepsy mutant mice with genetically disinhibited neural circuits (e.g., *GABRG2* mutations; ref. 50) could provide further insight. Because of the low spatial resolution of our 2-electrode DC recording, we could estimate the speed of propagation of SD to be the typical range (isolated SD: 2.19 ± 0.87 mm/min; SD in seizure+SD: 2.27 ± 0.83 mm/min), but not the propagation pattern of the SD wave. Imaging studies or a multi-electrode array may be needed to resolve this detail.

Our study detected SD events that outnumbered seizures in the adult *Scn1a*-deficient mouse model, and most of these SD events appeared in succession without a concurrent seizure. An earlier study that

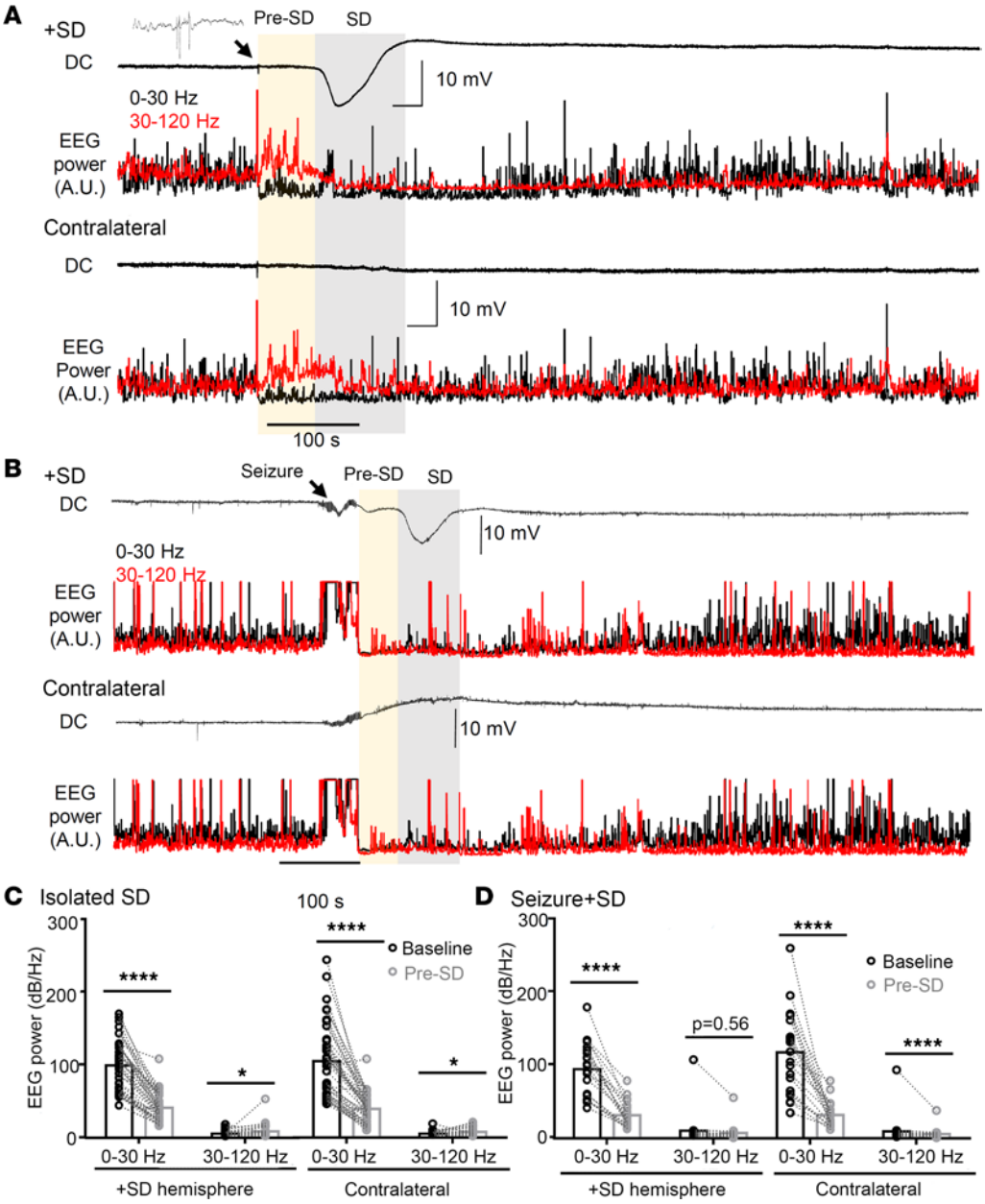

Figure 8. Prodromal EEG frequency change precedes the onset of the negative DC potential shift of SD. (**A**) DC and EEG power changes in isolated SD. EEG activities showed a robust high-frequency shift (yellow shade) more than a minute before the onset of the negative DC potential shift of SD. Note that complex EEG spikes are always detected at the onset of prodromal changes. DC, low-band (0–30 Hz, black), and high-band (30–120 Hz, red) EEG power in the SD-affected (top) and the contralateral hemisphere (bottom) are shown. (**B**) DC and EEG power changes during seizure+SD complex. (**C**) Quantification of the EEG power during baseline and prodromal phase from 45 isolated SDs. The EEG frequency was altered in both SD-affected and contralateral hemispheres (time effect: $P < 0.0001$ both hemispheres, repeated-measures ANOVA). (**D**) Same analysis of prodromal EEG frequency change in 21 seizure+SD complexes (time effect: $P < 0.001$ both hemispheres, repeated-measures ANOVA). *$P < 0.05$, ****$P < 0.001$, post hoc paired *t* test with Holm's correction.

suggested that SD may act as an antiseizure mechanism (51) was based mostly on the observation that SD transiently interrupts pharmacologically provoked ongoing EEG seizure discharges. We consider the mechanisms studied in that study more relevant to status epilepticus, rather than the spontaneous SD and seizure occurrence studied in this genetic epilepsy model, which is detected only a few times per day. Instead, we consider that the cortical activity state with SD and seizure represents a distinct disease profile as suggested by the consequence of hyperthermic seizure.

The frequent spontaneous SD waves detected in loss-of-function *Scn1a*-mutant mice described here may be counterintuitive, as they suggest a shared rather than opposite SD phenotype between loss- and gain-of-function mutant models. Our result rather suggests that SD might be commonly triggered in hyperexcitable epileptic brains even without a variant-specific mechanism, as SD can be readily triggered by external stimulation in the WT mouse cortex, while some mutations would certainly facilitate SD generation and create a unique phenotype as was seen in mice with *Kcnq2* conditional knockout (8). Similarly, the frequent SD in *Scn1a*$^{+/RX}$ mice seems contradictory to the observation that migraine with aura, generally considered to be an SD-linked neurological symptom, is not common in Dravet syndrome patients. Several possible explanations can be considered, including patient age (only 1%–3% of 7-year-old children experience migraine and the occurrence of aura without headache; ref. 52). The dissociation of these phenotypes may have several explanations: The pain threshold may be higher in Dravet syndrome because of a deficiency of peripheral *Scn1a*/Nav1.1 channels maintaining sensory nerve excitation (53), whereas FHM3-linked *Scn1a* gain-of-function mutations might reduce this threshold (54) and intensify headache sensation. FHM may represent a rare form of migraine linked to high SD susceptibility involving motor-related cortical regions, and SD generated in epilepsy may accompany distinct focal functional impairment depending on the affected brain region (55).

EEG signatures preceding spontaneous SD in Scn1a-deficient mice. We identified a prodromal high-frequency shift in EEG activity more than a minute before emergence of the negative DC potential shift in this model. Similar high-frequency activity preceding SD onset has been reported in SD evoked by potassium injection in anesthetized rat hippocampus (56). However, in that study, changes were detected only 5–10 seconds before onset of the negative DC potential shift and may not be directly comparable with the prodromal changes detected in this study. However, as in that study, we also identified complex EEG spikes at the onset of the pre-SD EEG pattern (Figure 8A, inset), which may possibly reflect a triggering mechanism for SD in this model.

In our recordings, more than 97% of spontaneous SD events were detected sequentially from the posterior to anterior electrodes, indicating a stereotypic SD generation pathway in this mouse. The result seems inconsistent with the known high anatomical SD susceptibility zone in the somatosensory barrel cortex in rodents (57, 58), which is located closer to the anterior electrodes. This discrepancy might indicate that spontaneous SD generation in *Scn1a*$^{+/RX}$ mice differs from that in the previous experimental SD models. Because of the limited spatial resolution in our chronic monitoring study, we could not pinpoint the spontaneous SD generation site more precisely. A microcircuit-based study of this mouse model may help identify an SD hotspot and better define the SD generation mechanism.

Our study also found that the duration of seizure activity during a seizure+SD complex is shorter than those in isolated seizure events. Given the stereotypic prodromal changes we found, the emergence of postictal SD may be somehow predetermined by this altered physiological state. We also identified a stereotyped delay in postictal SD onset, almost always 1 minute after seizure termination. This latency is in contrast with the *Kcnq2* conditional KO mouse model, where most SDs were bilateral and were generated even before seizure activity fully terminated (8). This result highlights the distinct SD regulatory mechanisms between epilepsy models with specific ion channel defects.

Aggravation of SD phenotype by a hyperthermic seizure. Febrile seizure due to infection or prolonged heat exposure is a common mechanism contributing to the onset and progression of Dravet syndrome (DS) symptoms, and similar hyperthermia-induced disease exacerbation is recapitulated in juvenile *Scn1a*-deficient mice (59, 60). Our observations are generally consistent with these earlier studies and further extend them by demonstrating that (a) a single brief seizure is sufficient to provoke an upsurge of SD, (b) seizure and SD exacerbation can occur in adult mice, and (c) the hyperthermic seizure effect can be prevented by concomitant memantine administration. This evidence suggests that the pathogenic mechanism of disease progression by a hyperthermic seizure may occur independently of critical developmental stages. In other words, the evolution of *Scn1a*-deficient encephalopathy may reflect sustained proexcitatory plasticity mechanisms rather than being solely determined by a static developmental defect. This view is consistent with studies demonstrating that postnatal conditional *Scn1a* deletion can create an epileptic encephalopathy similar to the genomic model (61, 62), and also that the disease phenotype can be reversed or ameliorated when *Scn1a* expression is recovered at a juvenile age (43, 63, 64).

The sustained proexcitatory effect of a hyperthermia-provoked seizure compared with the less consequential spontaneous seizure suggests an underlying functional difference between endogenously and exogenously triggered pathological excitation. In addition, 2 seizure-prone mice that had a reduced seizure frequency after

hyperthermic seizure (Figure 1) suggest that the effect of hyperthermic seizure could be altered in distinct disease conditions. Although the number is limited because of the rare chance to encounter these mice, they showed no SD during chronic monitoring and hyperthermic seizure. In addition to having recurrent seizures, increased SD threshold might correlate with the altered response to hyperthermic seizure.

Behavioral consequences of spontaneous SD. Our study also revealed that spontaneous SD is associated with motor behavior changes. SD was preceded by prodromal activation, and this motor behavior was later suppressed when SD invaded the frontal cortex (Figure 5). The latter is generally consistent with findings from optogenetically evoked SD in awake animals (40, 41). The seizure+SD complex also showed prolonged motor behavior suppression, which was occasionally detected as continuous immobility following PGES. A study in α2-Na^+/K^+-ATPase conditional KO mice described a paralyzing effect of putative cortical SD events (65). However, the paralytic state described in that study more closely resembled postictal coma than immobility. Postictal immobility has also been linked to the risk of severe respiratory dysfunction and sudden unexpected death in epilepsy (SUDEP) (31), a comorbidity in Dravet syndrome cases and mouse models. It will be important to examine whether the presence of postictal SD also modifies the cardiorespiratory consequences of seizure. Optogenetically evoked cortical SD can modify the heart rhythm in a sleep/awake status–dependent manner (ref. 40 and our unpublished observations).

Beyond the acute behavioral effect identified here, the early developmental and lasting effects of SD on the global neurological disorder remain to be elucidated. Previous studies suggest that recurrently provoked SD can injure synaptic biology, and incur chronic deficits associated with migraine with aura, such as hyperalgesia, photophobia, and anxiety (5, 6). In the current study design, we could not accurately measure these parameters, because such behavior tests interrupt the EEG recording and potentially affect the seizure/SD generation pattern. More controlled behavioral characterizations will be needed to understand the long-term contribution of spontaneous SD to neurological deficits associated with this developmental epileptic encephalopathy (DEE).

Benefits and limitations of memantine treatment. The demonstration that memantine can inhibit the hyperthermic seizure response (Figure 4) suggests a contribution of sustained NMDAR activation to the prolonged aftermath. Maximal suppression was found when memantine was administered before the hyperthermia episode. This effect is consistent with a recent randomized placebo-controlled clinical trial in which chronic memantine treatment reduced seizure frequency in pediatric developmental epileptic encephalopathy (DEE) patients (66). The prolonged suppression of SD/seizure frequency by memantine administration seen in our study suggests that memantine may have a potential role in DEE therapy when carefully administered.

On the other hand, we noted several *Scn1a*-deficient mice that displayed recurrent seizure activity during memantine administration, which resolved after the treatment. This response is probably related to reports of a paradoxical convulsive or excitatory effect of NMDAR inhibition. For example, acute NMDAR inhibition preferentially inhibits GABAergic interneurons (67), while chronic inhibition or depletion increases neuronal synaptic and intrinsic excitability (68–72), and some loss-of-function NMDAR mutations are associated with developmental epilepsy (73). Determining the lowest effective dose and slow escalation of the memantine dose may circumvent these events. A better understanding of the underlying cellular and molecular mechanisms linked to postictal sustained NMDAR activation, such as inflammation (74, 75) and neurotrophic signaling (76), may identify additional treatment options.

The present study identified a prominent SD phenotype and disturbed motor behavior associated with these depolarizing events in the *Scn1a*-deficient mouse model of Dravet syndrome. Together with our recent study of potassium channel–deficient mouse models of DEE (8), these findings suggest that SD may represent a neurological mechanism underlying the complex neurological deficits associated with genetic epileptic encephalopathy.

Methods

Animals. The *Scn1a*$^{+/R1407X}$ mice, originally developed in Kazuhiro Yamakawa's laboratory (21), were backcrossed with the heterozygote flox-tdTomato line (100% C57BL/6J background, Ai9, The Jackson Laboratory, 007909) and maintained on an 87.5% C57BL/6J and 12.5% SV129 background. The flox-tdTomato allele is inactive in the absence of Cre recombinase and was used as a post hoc label to blind the experimenter to genotype or treatment. Littermate WT mice were used as controls. During breeding and the chronic recording study, the mice had ad libitum access to mouse chow (5V5M, PicoLab) and drinking

water in rooms maintained at 20°C–24°C and 30%–50% humidity with a 12-hour light/12-hour dark cycle.

Surgery. Mice were injected with meloxicam (5 mg/kg, s.c.) as a presurgical analgesic, and anesthetized with isoflurane (3.0% induction, 1.5%–2.5% maintenance) while body temperature was maintained with a heating mat. The scalp hair was depilated and the skin cleansed with betadine and 70% ethanol 3 times. After injection of local anesthetics (1% lidocaine, 1% bupivacaine mixture), a midline skin incision was made to expose the skull surface, and connective tissues were removed with cotton swabs. Cranial burr holes (~1 mm diameter) were made 0.5 mm anterior/2.0 mm lateral and 2.5 mm posterior/2.5 mm lateral from the bregma and 2 burr holes in the occipital bone; the position occasionally required adjustment by about 0.5 mm when major blood vessels were present. In each burr hole, a drop of dexamethasone (10 mg/mL) was topically applied to ameliorate tissue inflammation. Teflon-insulated silver wires (36 gauge or ~0.13 mm diameter) were carefully positioned over the cortical surface, and a pair of wires were inserted under the neck muscles for electromyogram (EMG) recording. After implantation, the wires and connector were cemented to the skull with Metabond (Parkell). Mice received meloxicam (5 mg/kg) for 3 postoperative days. To minimize the postsurgical effect, EEG recordings were initiated at least 7 days after the implant.

Video EEG recording of awake mice. EEG recordings were conducted in an IACUC-approved satellite room (20°C–22°C, 40% humidity, 12-hour light/12-hour dark cycle). Each mouse was connected to an EEG tether wire and housed in a 30 × 15 cm home cage with freely available water and food. To minimize the potential influence of exposure to a new environment, activity recorded during the first 48 hours in the cage was excluded from the analysis. EEG activity was acquired using a Bioamp DC amplifier at 1 kHz and digitized by the LabChart system (ADI) while the behavior was continuously recorded using an infrared light–equipped complementary metal-oxide-semiconductor (CMOS) camera (Ailipu Technology) at 2 Hz. EEG signals were analyzed using LabChart (ADI) and Clampfit 10 software (Molecular Devices). The use of DC-compatible amplifiers was necessary for SD detection by cortical surface EEG recording as slow signals are filtered out in most AC-coupled amplifiers.

All raw EEG traces were visually inspected for seizure and SD incidence and were manually quantified based on their characteristic EEG patterns as described in our previous study (8). Postictal generalized EEG suppression (PGES) was defined as the complete suppression of EEG amplitude immediately after seizure termination, and the duration was determined based on the total EEG power (total EEG power < 0.01 mV^2; see Figure 3A). In the EEG analysis in Figure 8, the total power of low-frequency (0–30 Hz) and high-frequency band (30–120 Hz) cortical activities was calculated by fast Fourier transformation (N = 1,024, cosine-bell waveform).

The video image was analyzed using Bonsai and R software. Locomotion was calculated based on the horizontal displacement of the mouse body centroid. Some video images were excluded from the analysis because the mouse position could not be accurately resolved. The peaks of EEG event incidences in the circadian phase were obtained by the creation of a density plot.

Induction of hyperthermic seizure. After baseline recording, the mice were transferred to a glass-walled chamber equipped with a combined heating lamp and cooling mat. These experiments were conducted between 11:00 am and 12:30 pm. Hyperthermia was induced using a heating lamp while cortical EEG and body temperature were continuously monitored. As soon as a seizure was detected, the mouse was placed on an iced mat to cool the body to 37°C, then returned to the recording cage where EEG monitoring was continued. The body cooling was used to improve clinical recovery from hyperthermia; however, SD incidence during hyperthermia in *Scn1a*$^{+/RX}$ mice was also observed in initial studies without body cooling.

Drug. Memantine was purchased from Tocris, and PTZ was obtained from MilliporeSigma. Both drugs were dissolved in saline on the day of the experiment and administered by i.p. injection.

Study design and statistics. EEG recording studies included both male and female *Scn1a*$^{R1407X/+}$ and *Scn1a*$^{+/+}$ WT littermates in each cohort. Two to four mice were simultaneously recorded in each study cohort. Because some littermate mutant mice died or became moribund during the study, we added several *Scn1a*^{RX} mice, resulting in an unequal number of mice by sex. Cage location and order of treatments were randomly assigned, and the experimenters were blinded to genotype when possible.

The number of animals in the initial characterization was determined based on power analysis. The numbers of animals in the memantine and PTZ studies were determined based on the results of the initial cohort.

Statistics were calculated by R and GraphPad Prism software. Because most of the data showed skewed distribution, statistical significance was tested using non-parametric methods such as aligned rank transfor-

mation ANOVA for multiple comparisons (77), Wilcoxon's signed-rank test, and Mann-Whitney *U* test for 2-sample comparisons. All 2-group comparisons were 2-tailed. A *P* value less than 0.05 was considered significant. The data are presented as mean ± SD unless otherwise specified in the figure legends.

Study approval. All animal experiments were conducted according to the guide of the Association for Assessment and Accreditation of Laboratory Animal Care International (AAALAC) and approved by the IACUC of Baylor College of Medicine.

Data availability. The raw data of this study are included in the Supporting Data Values (available online with this article; https://doi.org/10.1172/jci.insight.170399DS1). All electrophysiological and imaging data are available upon request.

Author contributions

IA conceived and designed the study. IA and YN acquired and analyzed data. IA and JLN drafted the manuscript. All authors contributed to the final draft of the manuscript.

Acknowledgments

This work was supported by American Heart Association Career Development Grant 19CDA34660056 (to IA), the Curtis Hankamer Basic Research Fund at Baylor College of Medicine (to IA), an American Epilepsy Society Junior Investigator Award (to IA), National Institutes of Health Center for SUDEP Research Grant NS090340 (to JLN), and the Blue Bird Circle Foundation (to JLN).

Address correspondence to: Isamu Aiba, Department of Neurology, Baylor College of Medicine, One Baylor Plaza, Houston, Texas 77030, USA. Phone: 713.798.5862; Email: aiba@bcm.edu.

1. Somjen GG. Mechanisms of spreading depression and hypoxic spreading depression-like depolarization. *Physiol Rev*. 2001;81(3):1065–1096.
2. Dreier JP. The role of spreading depression, spreading depolarization and spreading ischemia in neurological disease. *Nat Med*. 2011;17(4):439–447.
3. Major S, et al. Direct electrophysiological evidence that spreading depolarization-induced spreading depression is the pathophysiological correlate of the migraine aura and a review of the spreading depolarization continuum of acute neuronal mass injury. *Geroscience*. 2020;42(1):57–80.
4. Ayata C. Cortical spreading depression triggers migraine attack: pro. *Headache*. 2010;50(4):725–730.
5. Harriott AM, et al. Optogenetic spreading depression elicits trigeminal pain and anxiety behavior. *Ann Neurol*. 2020;89(1):99–110.
6. Tang C, et al. Cortical spreading depolarisation-induced facial hyperalgesia, photophobia and hypomotility are ameliorated by sumatriptan and olcegepant. *Sci Rep*. 2020;10(1):11408.
7. Dreier JP, et al. Spreading convulsions, spreading depolarization and epileptogenesis in human cerebral cortex. *Brain*. 2012;135(pt 1):259–275.
8. Aiba I, Noebels JL. Kcnq2/Kv7.2 controls the threshold and bi-hemispheric symmetry of cortical spreading depolarization. *Brain*. 2021;144(9):2863–2878.
9. Rogawski MA. Migraine and epilepsy—shared mechanisms within the family of episodic disorders. In: Noebels JL, et al., eds. *Jasper's Basic Mechanisms of the Epilepsies*. National Center for Biotechnology Information; 2012:930–944.
10. Aiba I, Noebels JL. Spreading depolarization in the brainstem mediates sudden cardiorespiratory arrest in mouse SUDEP models. *Sci Transl Med*. 2015;7(282):282ra46.
11. Loonen ICM, et al. Brainstem spreading depolarization and cortical dynamics during fatal seizures in Cacna1a S218L mice. *Brain*. 2019;142(2):412–425.
12. Eikermann-Haerter K, et al. Enhanced subcortical spreading depression in familial hemiplegic migraine type 1 mutant mice. *J Neurosci*. 2011;31(15):5755–5763.
13. Foreman B, et al. The relationship between seizures and spreading depolarizations in patients with severe traumatic brain injury. *Neurocrit Care*. 2022;37(suppl 1):31–48.
14. Wang W, Frankel WN. Overlaps, gaps, and complexities of mouse models of developmental and epileptic encephalopathy. *Neurobiol Dis*. 2021;148:105220.
15. Symonds JD, et al. Incidence and phenotypes of childhood-onset genetic epilepsies: a prospective population-based national cohort. *Brain*. 2019;142(8):2303–2318.
16. Ding J, et al. SCN1A mutation-beyond Dravet syndrome: a systematic review and narrative synthesis. *Front Neurol*. 2021;12:743726.
17. Ogiwara I, et al. Nav1.1 haploinsufficiency in excitatory neurons ameliorates seizure-associated sudden death in a mouse model of Dravet syndrome. *Hum Mol Genet*. 2013;22(23):4784–4804.
18. Yamagata T, et al. Scn1a -GFP transgenic mouse revealed Nav1.1 expression in neocortical pyramidal tract projection neurons. *Elife*. 2023;12:e87495.
19. Smith RS, et al. Sodium channel SCN3A ($Na_V1.3$) regulation of human cerebral cortical folding and oral motor development. *Neuron*. 2018;99(5):905–913.

20. Yu FH, et al. Reduced sodium current in GABAergic interneurons in a mouse model of severe myoclonic epilepsy in infancy. *Nat Neurosci*. 2006;9(9):1142–1149.
21. Ogiwara I, et al. Nav1.1 localizes to axons of parvalbumin-positive inhibitory interneurons: a circuit basis for epileptic seizures in mice carrying an Scn1a gene mutation. *J Neurosci*. 2007;27(22):5903–5914.
22. Rosch RE, Goldberg EM. SCN1A and Dravet syndrome. In: Baram TZ, et al., eds. *Febrile Seizures: New Concepts and Consequences.* 2nd ed. Elsevier; 2023:43–63.
23. Clatot J, et al. SCN1A gain-of-function mutation causing an early onset epileptic encephalopathy. *Epilepsia*. 2023;64(5):1318–1330.
24. Brunklaus A, et al. The gain of function SCN1A disorder spectrum: novel epilepsy phenotypes and therapeutic implications. *Brain*. 2022;145(11):3816–3831.
25. Auffenberg E, et al. Hyperexcitable interneurons trigger cortical spreading depression in an Scn1a migraine model. *J Clin Invest*. 2021;131(21):e142202.
26. Jansen NA, et al. First FHM3 mouse model shows spontaneous cortical spreading depolarizations. *Ann Clin Transl Neurol*. 2020;7(1):132–138.
27. Catterall WA, et al. NaV1.1 channels and epilepsy. *J Physiol*. 2010;588(pt 11):1849–1859.
28. Connolly MB. Dravet syndrome: diagnosis and long-term course. *Can J Neurol Sci*. 2016;43(s3):S3–S8.
29. Teran FA, et al. Time of day and a ketogenic diet influence susceptibility to SUDEP in Scn1a $^{R1407X/+}$ mice. *Front Neurol*. 2019;10:278.
30. Oakley JC, et al. Temperature- and age-dependent seizures in a mouse model of severe myoclonic epilepsy in infancy. *Proc Natl Acad Sci U S A*. 2009;106(10):3994–3999.
31. Kuo J, et al. Postictal immobility and generalized EEG suppression are associated with the severity of respiratory dysfunction. *Epilepsia*. 2016;57(3):412–417.
32. Moseley BD, et al. Characteristics of postictal generalized EEG suppression in children. *Epilepsy Res*. 2013;106(1–2):123–127.
33. Morimoto T, et al. The pathogenic role of the NMDA receptor in hyperthermia-induced seizures in developing rats. *Brain Res Dev Brain Res*. 1995;84(2):204–207.
34. Beconi MG, et al. Pharmacokinetics of memantine in rats and mice. *PLoS Curr*. 2011;3:RRN1291.
35. Creeley C, et al. Low doses of memantine disrupt memory in adult rats. *J Neurosci*. 2006;26(15):3923–3932.
36. Peeters M, et al. Effects of pan- and subtype-selective N-methyl-D-aspartate receptor antagonists on cortical spreading depression in the rat: therapeutic potential for migraine. *J Pharmacol Exp Ther*. 2007;321(2):564–572.
37. Yuskaitis CJ, et al. Factors influencing the acute pentylenetetrazole-induced seizure paradigm and a literature review. *Ann Clin Transl Neurol*. 2021;8(7):1388–1397.
38. Jun HW. Pharmacokinetic studies of pentylenetetrazol in dogs. *J Pharm Sci*. 1976;65(7):1038–1041.
39. Petrucci AN, et al. Post-ictal generalized EEG suppression is reduced by enhancing dorsal raphe serotonergic neurotransmission. *Neuroscience*. 2021;453:206–221.
40. Yousef Yengej D, et al. Different characteristics of cortical spreading depression in the sleep and wake states. *Headache*. 2022;62(5):577–587.
41. Houben T, et al. Optogenetic induction of cortical spreading depression in anesthetized and freely behaving mice. *J Cereb Blood Flow Metab*. 2017;37(5):1641–1655.
42. Ito S, et al. Mouse with Nav1.1 haploinsufficiency, a model for Dravet syndrome, exhibits lowered sociability and learning impairment. *Neurobiol Dis*. 2013;49:29–40.
43. Valassina N, et al. Scn1a gene reactivation after symptom onset rescues pathological phenotypes in a mouse model of Dravet syndrome. *Nat Commun*. 2022;13(1):161.
44. Fadila S, et al. Convulsive seizures and some behavioral comorbidities are uncoupled in the Scn1a^{A1783V} Dravet syndrome mouse model. *Epilepsia*. 2020;61(10):2289–2300.
45. Han S, et al. Autistic-like behaviour in Scn1a+/- mice and rescue by enhanced GABA-mediated neurotransmission. *Nature*. 2012;489(7416):385–390.
46. Tran CH, et al. Interneuron desynchronization precedes seizures in a mouse model of Dravet syndrome. *J Neurosci*. 2020;40(13):2764–2775.
47. Schiefecker AJ, et al. Brain temperature but not core temperature increases during spreading depolarizations in patients with spontaneous intracerebral hemorrhage. *J Cereb Blood Flow Metab*. 2018;38(3):549–558.
48. Wu J, Fisher RS. Hyperthermic spreading depressions in the immature rat hippocampal slice. *J Neurophysiol*. 2000;84(3):1355–1360.
49. Parker PD, et al. Non-canonical glutamate signaling in a genetic model of migraine with aura. *Neuron*. 2021;109(4):611–628.
50. Kang J-Q, Macdonald RL. Molecular pathogenic basis for GABRG2 mutations associated with a spectrum of epilepsy syndromes, from generalized absence epilepsy to Dravet syndrome. *JAMA Neurol*. 2016;73(8):1009–1016.
51. Tamim I, et al. Spreading depression as an innate antiseizure mechanism. *Nat Commun*. 2021;12(1):2206.
52. Barnes N, et al. Migraine headache in children. *BMJ Clin Evid*. 2006;2015(15):469–475.
53. Espino CM, et al. NaV1.1 is essential for proprioceptive signaling and motor behaviors. *Elife*. 2022;11:e79917.
54. Suleimanova A, et al. Deciphering in silico the role of mutated Na_v1.1 sodium channels in enhancing trigeminal nociception in familial hemiplegic migraine type 3. *Front Cell Neurosci*. 2021;15:644047.
55. Pietrobon D, Moskowitz MA. Chaos and commotion in the wake of cortical spreading depression and spreading depolarizations. *Nat Rev Neurosci*. 2014;15(6):379–393.
56. Herreras O, et al. Role of neuronal synchronizing mechanisms in the propagation of spreading depression in the in vivo hippocampus. *J Neurosci*. 1994;14(11 pt 2):7087–7098.
57. Bogdanov VB, et al. Susceptibility of primary sensory cortex to spreading depolarizations. *J Neurosci*. 2016;36(17):4733–4743.
58. Juzekaeva E, et al. Preferential initiation and spread of anoxic depolarization in layer 4 of rat barrel cortex. *Front Cell Neurosci*. 2017;11:390.
59. Salgueiro-Pereira AR, et al. A two-hit story: seizures and genetic mutation interaction sets phenotype severity in SCN1A epilepsies. *Neurobiol Dis*. 2019;125:31–44.

60. Dutton SBB, et al. Early-life febrile seizures worsen adult phenotypes in Scn1a mutants. *Exp Neurol*. 2017;293:159–171.
61. Stein RE, et al. Hippocampal deletion of $Na_V1.1$ channels in mice causes thermal seizures and cognitive deficit characteristic of Dravet syndrome. *Proc Natl Acad Sci U S A*. 2019;116(33):16571–16576.
62. Jansen NA, et al. Focal and generalized seizure activity after local hippocampal or cortical ablation of $Na_V1.1$ channels in mice. *Epilepsia*. 2020;61(4):e30–e36.
63. Yamagata T, et al. CRISPR/dCas9-based Scn1a gene activation in inhibitory neurons ameliorates epileptic and behavioral phenotypes of Dravet syndrome model mice. *Neurobiol Dis*. 2020;141:104954.
64. Tanenhaus A, et al. Cell-selective adeno-associated virus-mediated SCN1A gene regulation therapy rescues mortality and seizure phenotypes in a Dravet syndrome mouse model and is well tolerated in nonhuman primates. *Hum Gene Ther*. 2022;33(11–12):579–597.
65. Smith SE, et al. Astrocyte deletion of α2-Na/K ATPase triggers episodic motor paralysis in mice via a metabolic pathway. *Nat Commun*. 2020;11(1):6164.
66. Schiller K, et al. Randomized placebo-controlled crossover trial of memantine in children with epileptic encephalopathy. *Brain*. 2023;146(3):873–879.
67. Homayoun H, Moghaddam B. NMDA receptor hypofunction produces opposite effects on prefrontal cortex interneurons and pyramidal neurons. *J Neurosci*. 2007;27(43):11496–11500.
68. Lüthi A, et al. NMDA receptor activation limits the number of synaptic connections during hippocampal development. *Nat Neurosci*. 2001;4(11):1102–1107.
69. Fukushima F, et al. Ablation of NMDA receptors enhances the excitability of hippocampal CA3 neurons. *PLoS One*. 2009;4(1):e3993.
70. Tatard-Leitman VM, et al. Pyramidal cell selective ablation of N-methyl-D-aspartate receptor 1 causes increase in cellular and network excitability. *Biol Psychiatry*. 2015;77(6):556–568.
71. Hou G, Zhang Z-W. NMDA receptors regulate the development of neuronal intrinsic excitability through cell-autonomous mechanisms. *Front Cell Neurosci*. 2017;11:353.
72. He S, et al. Synaptic and extrasynaptic plasticity in glutamatergic circuits involving dentate granule cells following chronic N-methyl-D-aspartate receptor inhibition. *J Neurophysiol*. 2013;109(6):1535–1547.
73. XiangWei W, et al. De novo mutations and rare variants occurring in NMDA receptors. *Curr Opin Physiol*. 2018;2:27–35.
74. Dubé CM, et al. Epileptogenesis provoked by prolonged experimental febrile seizures: mechanisms and biomarkers. *J Neurosci*. 2010;30(22):7484–7494.
75. Wu L-J. Upregulation of forebrain NMDA NR2B receptors contributes to behavioral sensitization after inflammation. *J Neurosci*. 2005;25(48):11107–11116.
76. Kim YH, et al. The induction of BDNF and c-fos mRNA in the hippocampal formation after febrile seizures. *Neuroreport*. 2001;12(15):3243–3246.
77. Wobbrock JO, et al. The aligned rank transform for nonparametric factorial analyses using only anova procedures. CHI '11: Proceedings of the SIGCHI Conference on Human Factors in Computing Systems. Association for Computing Machinery. 2011;143–146. https://dl.acm.org/doi/10.1145/1978942.1978963. Accessed June 21, 2023.